nature chemistry

Article

https://doi.org/10.1038/s41557-023-01303-0

Quantum simulation of conical intersections using trapped ions

In the format provided by the authors and unedited

SUPPLEMENTARY MATERIAL

Table of Contents

1. Supplementary Note 1: Mapping to the Trapped Ion Hamiltonian

2. Supplementary Note 2: Effect of Off-Resonant Coupling on Measurement

3. Supplementary Note 3: Sensitivity to Noise

4. Supplementary Note 4: Justification of Different Evolution

Supplementary Note 1: Mapping to the Trapped Ion Hamiltonian

Much of the material in this section follows the work of [1]. We start with one ion, but the extension to multiple ions is fairly obvious. Ignoring the unused axial mode (which is perpendicular to the beams and therefore not coupled into), the one ion Hamiltonian can be written as follows:

$$\hat{H}_{ion} = \frac{\omega_0}{2}\hat{\sigma}_z + \nu_x\hat{n}_x + \nu_y\hat{n}_y + \hat{H}^{(i)}, \tag{1}$$

where ω_0 is the energy difference between chosen qubit states, and ν_x and ν_y are the vibrational frequencies of the x and y modes, respectively. Here, the motion of the ion has been approximated as a harmonic oscillator, which is a reasonable assumption if the micromotion caused by the RF drive frequency can be ignored. The interaction between the motional modes and the electronic states of the ion, mediated via four different lasers, is:

$$\hat{H}^{(i)} = \sum_{\substack{\text{j=1,2}\\ \text{q = x,y}}} \frac{\Omega_{j,q}}{2}\sigma_x\big(e^{i(k_{j,q}\hat{q}-\omega_{j,q}t+\phi_{j,q})} + h.c.\big), \tag{2}$$

where $\Omega_{j,q}$, $k_{j,q}$, $\omega_{j,q}$, $\phi_{j,q}$ are the electric field strength, wave vector, frequency, and phase of the jth beam intended to couple into mode q. Here, two of the lasers interact with the x motion of the ion and the other two interact with the y motion. Moving into the interaction picture, and performing the rotating wave approximation, we get the following Hamiltonian:

$$\hat{H}_{int} = e^{-i\hat{H}_0 t}\hat{H}^{(i)}e^{i\hat{H}_0 t} \approx \sum_{\substack{\text{j=1,2}\\ \text{q = x,y}}} \frac{\Omega_{j,q}}{2}\hat{\sigma}_+ \exp\left(i(\eta_{j,q}[\hat{a}_q e^{-i\nu_q t} + \hat{a}_q^\dagger e^{i\nu_q t}] - \delta_{j,q}t + \phi_{j,q})\right) + h.c., \tag{3}$$

where $\hat{H}_0 = \hat{H}_{ion} - \hat{H}^{(i)}$ is the diagonal part of the total Hamiltonian, $\delta_{j,q}$ is the detuning between the laser and qubit resonance, and $\eta_{j,q}$ is the Lamb-Dicke parameter taking into account the motional coupling between the laser and the ion. In the Lamb-Dicke regime, i.e. $\eta\langle 2n+1\rangle \ll 1$, we can approximate the exponential operators to the first order, leaving us with the following approximate interaction Hamiltonian:

$$\hat{H}_{int} \approx \sum_{\substack{\text{j=1,2}\\ \text{q = x,y}}} \frac{\Omega_{j,q}}{2}\hat{\sigma}_+(1 + i\eta_{j,q}(\hat{a}_q e^{-i\nu_q t} + \hat{a}_q^\dagger e^{i\nu_q t}))e^{i(-\delta_{j,q}t+\phi_{j,q})} + h.c. \tag{4}$$

If we properly set the phase and detuning of each of our lasers, and perform a second rotating wave approximation, we can obtain the following Hamiltonian:

$$\hat{H}_{int} \approx \frac{\eta\Omega}{2}\Big(\hat{\sigma}_x(\hat{a}_x e^{-i\nu t} + \hat{a}_x^\dagger e^{i\nu t}) + \hat{\sigma}_y(\hat{a}_y e^{-i\nu t} + \hat{a}_y^\dagger e^{i\nu t})\Big). \tag{5}$$

This is clearly very close to the desired Hamiltonian in Eq. 7 in the main text. All that remains is to rotate slightly out of the full interaction picture with a number operators in both modes proportional to ν. The result is the following effective Hamiltonian:

$$\hat{H}_{eff} \approx \nu(\hat{n}_x + \hat{n}_y) + \frac{\eta\Omega}{2}\Big(\hat{\sigma}_x(\hat{a}_x + \hat{a}_x^\dagger) + \hat{\sigma}_y(\hat{a}_y + \hat{a}_y^\dagger)\Big). \tag{6}$$

This is exactly what we want. Unfortunately we have made several approximations to obtain this result. To account for these during classical simulation of our experiment, we used the following less approximate Hamiltonian instead:

$$\begin{aligned}\hat{H}_{noisy} \approx & \frac{\Delta_z}{2}\hat{\sigma}_z + \nu(\hat{n}_x + \hat{n}_y) + \\ & (\frac{\eta\Omega}{2})\Big(\hat{\sigma}_x(\hat{a}_x + \hat{a}_x^\dagger) + \hat{\sigma}_y(\hat{a}_y + \hat{a}_y^\dagger) + \hat{\sigma}_x((\hat{a}_y + \hat{a}_y^\dagger)\cos(\Delta_{xy}t) + \\ & i(\hat{a}_y - \hat{a}_y^\dagger)\sin(\Delta_{xy}t)) + \hat{\sigma}_y((\hat{a}_x + \hat{a}_x^\dagger)\cos(\Delta_{xy}t) - i(\hat{a}_x - \hat{a}_x^\dagger)\sin(\Delta_{xy}t))\Big).\end{aligned} \tag{7}$$

This takes into account improper detuning in our lasers via Δ_z, as well as any cross coupling between lasers meant for the x mode with the y mode, and vice versa, where Δ_{xy} is the frequency difference between the modes. This noise was approximated away via the second rotating wave approximation we made. Lastly, we took into account heating and phase noise caused by micro-motion and other sources by plugging this Hamiltonian into the full Lindblad master equation, $\dot{\rho} = \frac{1}{i}\big[\hat{H}_{noisy}, \rho\big] + \frac{1}{2}\sum_j \gamma_j(2L_j\rho L_j^\dagger - L_j^\dagger L_j\rho - \rho L_j^\dagger L_j)$, where $L_j \in \{\hat{a}_x, \hat{a}_x^\dagger, \hat{n}_x, \hat{a}_y, \hat{a}_y^\dagger, \hat{n}_y\}$.

Supplementary Note 2: Effect of Off-Resonant Coupling on Measurement

When extending equations like Eq. 4 to multiple ions, the main difference is to add one spin term and two motional modes per ion (once again ignoring axial modes for the same reason). The extra spin terms can be ignored because we have individual addressing of ions. The extra motional modes can also be ignored up to the rotating wave approximation. This is not always accurate

however, because motional modes can bunch together as the number of ions grow. In our five ion chain, we used one of the nearest neighbors of the center ion to measure the normal mode distributions of the ions. This ion couples to all modes, unlike the center ion that we used for the adiabatic evolution, which only coupled to every other mode [2, 3]. The frequency difference for each modes was about $2\pi\times$ 30-50 kHz, compared to a Rabi frequency of about $2\pi\times$ 3-5 kHz, and we need to include off-resonant effects on the "Fourier-Push". We start by including one extra mode, using the following effective Hamiltonian:

$$H = \frac{\eta_1\Omega}{2}\sigma_x(a_1 + a_1^\dagger) + \frac{\eta_2\Omega}{2}\sigma_x(a_2 e^{-i\Delta t} + a_2^\dagger e^{i\Delta t}), \tag{8}$$

where η_1 and η_2 are the Lamb-Dicke parameters for the two respective modes, Ω is the carrier Rabi frequency, Δ is the detuning from mode 2, and we are trying to measure mode 1. We note from [4] that for any Hamiltonian that can be written as $i(\gamma(t)a - \gamma^*(t)a^\dagger)\mathcal{O}$, the unitary evolution is $U(t) = \hat{D}(\alpha(t)\mathcal{O})\exp(i\Phi(t)\mathcal{O}^2)$, where $\hat{D}$ is the displacement operator, $\alpha(t) = \int_0^t dt'\gamma(t')$, $\Phi(t) = \mathrm{Im}[\int_0^t dt'\gamma(t')\int_0^{t'} dt''\gamma(t'')]$, and $\mathcal{O}$ is any arbitrary operator. In our case, $\mathcal{O} = \sigma_x$, and therefore $\mathcal{O}^2$ is the identity, so the second term is simply a global phase we can ignore. The two parts of the Hamiltonian that couple into different modes commute, so we can write the unitary evolution as:

$$U(t) = \exp\big(\frac{-i\eta_1\Omega t}{2}\sigma_x(a_1 + a_1^\dagger)\big)\exp\big(-i\frac{\eta_2\Omega}{\Delta}\sin(\Delta t/2)\sigma_x(a_2 e^{-i\Delta/2} + a_2^\dagger e^{i\Delta/2})\big). \tag{9}$$

By expanding the exponential operator, we reach the following expectation for our σ_z projection measurement:

$$\begin{aligned}
&\langle U(t)^\dagger\sigma_z U(t)\rangle = \\
&\langle\sigma_z\big(\cos(\sqrt{2}\eta_1\Omega t x_1)\cos(2\sqrt{2}\frac{\eta_2\Omega}{\Delta}\sin(\Delta t/2)(x_2\cos(\Delta t/2) + p_2\sin(\Delta t/2))) \\
&+ \sin(\sqrt{2}\eta_1\Omega t x_1)\sin(2\sqrt{2}\frac{\eta_2\Omega}{\Delta}\sin(\Delta t/2)(x_2\cos(\Delta t/2) + p_2\sin(\Delta t/2)))\big)\rangle + \\
&\langle\sigma_y\big(\cos(\sqrt{2}\eta_1\Omega t x_1)\sin(2\sqrt{2}\frac{\eta_2\Omega}{\Delta}\sin(\Delta t/2)(x_2\cos(\Delta t/2) + p_2\sin(\Delta t/2))) \\
&+ \sin(\sqrt{2}\eta_1\Omega t x_1)\cos(2\sqrt{2}\frac{\eta_2\Omega}{\Delta}\sin(\Delta t/2)(x_2\cos(\Delta t/2) + p_2\sin(\Delta t/2)))\big)\rangle.
\end{aligned} \tag{10}$$

We see that we are essentially taking a secondary Fourier transform at this point, except with an oscillating k-number. This has the effect of modulating the original signal. At this point, we make the approximation that the off-resonant mode is in a thermal state. This helps us in two ways,

first by removing any odd portions of new modulating terms, and second by allowing us to ignore any difference between x_2 and p_2. The new expectation value is:

$$\begin{aligned}\langle U(t)^\dagger \sigma_z U(t)\rangle &= \langle \cos(2\sqrt{2}\frac{\eta_2\Omega}{\Delta}\sin(\Delta t/2)x_2)\big(\sigma_z\cos(\sqrt{2}\eta_1\Omega t x_1)+\sigma_y\sin(\sqrt{2}\eta_1\Omega t x_1)\big)\rangle \\ &= \int dx_1 dx_2 |\psi_1(x_1)|^2|\psi_2(x_2)|^2\cos(2\sqrt{2}\frac{\eta_2\Omega}{\Delta}\sin(\Delta t/2)x_2)\big(\langle\sigma_z\rangle\cos(\sqrt{2}\eta_1\Omega t x_1)+\langle\sigma_y\rangle\sin(\sqrt{2}\eta_1\Omega t x_1)\big).\end{aligned} \tag{11}$$

Because it's in a thermal state, we assume that $|\psi_2(x_2)|^2 \propto \exp(-x_2^2/2\sigma^2)$ where σ depends on how well cooled the mode is. By performing the Fourier transform, we get:

$$\begin{aligned}&\langle U(t)^\dagger \sigma_z U(t)\rangle = \\ &\int dx_1 |\psi_1(x_1)|^2 \exp(-4\sigma^2\frac{\eta_2^2\Omega^2}{\Delta^2}\sin^2(\frac{\Delta t}{2}))\big(\langle\sigma_z\rangle\cos(\sqrt{2}\eta_1\Omega t x_1)+\langle\sigma_y\rangle\sin(\sqrt{2}\eta_1\Omega t x_1)\big).\end{aligned} \tag{12}$$

We see that the signal is modulated by a Gaussian-like wave-packet, except the argument is a sine function. The effect of this is to add Gaussian noise to the inverse Fourier transform (which in turn appears to be a large thermal background). In theory, the signal could be demodulated if the exact parameters of $|\psi_2(x_2)|^2$ are known, but this is difficult enough for one extra mode and in one dimension. In our experiment, the measurement in the effective x-direction is close enough to one mode to be affected, while the measurement of the y-direction is close enough to two modes. The final signal would have to be demodulated in three different ways.

Supplementary Note 3: Sensitivity to Noise

While the one ion case is intuitive to map to for this experiment, it is not as resistant to noise as a multi ion simulation [5, 6]. Heating rates in the center of mass modes of ion chains tend to be higher than those of other modes ($>$ 100 quanta/sec in our set up), and the only mode available to a single ion simulation is the center of mass mode. With two ions, we have the tilt mode available in the x and y axes, which corresponds to the ions oscillating exactly out of phase with each other and can have a heating rate as low as an order of magnitude smaller than that of the center of mass mode.

With a five ion setup, we have even less sensitive modes to utilize [2, 3]. The best is the zigzag mode, which corresponds to nearest neighbor ions moving out of phase with each other. Due to our choice of ions to use (the middle ion and the one directly to the left), the next best available mode is the so-called third mode, which corresponds to the middle three ions moving out of phase

with the edge ions. Both of these modes have measured heating rates of less than one per second, and motional dephasing times on the order of 8 ms in our system, much longer than our adiabatic evolution.

Supplementary Note 4: Justification of Different Evolution

The natural choice of path around the conical intersection would be to first push the wavefunction out to the desired radius with a spin-dependent laser force in the x-mode, followed by a spin-dependent laser force that opens up the path around the intersection with the y-mode. This can be described temporally by:

$$\hat{H}(t) = \nu\hat{n}_x + \nu\hat{n}_y + \left\{ \begin{array}{ll} \frac{\Omega t}{2\tau}\hat{\sigma}_x(\hat{a}_x + \hat{a}_x^\dagger), & \text{if } 0 \leq t \leq \tau \\ \frac{\Omega}{2}\hat{\sigma}_x(\hat{a}_x + \hat{a}_x^\dagger) + \frac{\Omega(t-\tau)}{2\tau}\hat{\sigma}_y(\hat{a}_y + \hat{a}_y^\dagger), & \text{if } \tau < t \leq 2\tau \end{array} \right\} \tag{13}$$

Due to the perfect circle of the path taken by the wavefunction, the argument of geometric phase interference is very clean. Instead, we turn on both the x-mode interaction and the y-mode interaction at the same time, as described in Eq. 8 in the main text. This immediately brings in the argument that by starting at the degeneracy point, or the point where the notion of adiabaticity makes no sense, we invalidate one of the key requirements of geometric phase. Our intuitive argument that this still produces geometric phase interference is that by starting in the $|+\rangle$ state, we have broken a symmetry. This pushes the ion to the negative direction in the x-mode in the beginning. After that, the conical intersection is still at the center of the potential energy surface, and the whole wavefunction is still in the ground state of the Hamiltonian. Thus, from this point onward, all the normal arguments apply, and the only thing stopping the ion from spreading to the other side over time has to be a geometric phase, because the dynamic phase on the wavefunction is the same for all positions.

More rigorously, we note the following equations of motion given by the dynamics of the Hamiltonian:

$$\begin{aligned} \langle \ddot{x} \rangle &= -\nu^2 \langle x \rangle - \frac{\Omega\nu t}{\sqrt{2}\tau} \langle \sigma_x \rangle , \\ \langle \ddot{y} \rangle &= -\nu^2 \langle y \rangle - \frac{\Omega\nu t}{\sqrt{2}\tau} \langle \sigma_y \rangle . \end{aligned} \tag{14}$$

For very small times, $\langle \sigma_x \rangle \approx 1$ and thus $\nu |\langle x \rangle| \ll \frac{\Omega}{2} |\langle \sigma_x \rangle|$, meaning there's an initial push in the negative direction of the whole wavefunction of about $\langle x \rangle \approx -\frac{\nu\Omega}{2\sqrt{2}} t^2$. By mapping $x + iy = z$,

we can perform a contour integral and utilize the residue theorem. This is particularly convenient because Eq. 5 in the main text takes the form:

$$\gamma_{\pm} = \frac{1}{4i}\int_{z_0}^{z_f} (\frac{dz}{z} - \frac{dz^*}{z^*}). \tag{15}$$

This integral famously evaluates to $\pm\pi$ if it makes a loop around the singularity at the center point $z = 0$, depending on the direction of travel, and evaluates to $\pm\frac{\pi}{2}$ if it travels exactly halfway around the singularity. Based on our initial push in the negative direction, our parameterization can roughly be written as $x = \cos(\theta) + \epsilon$ and $y = \sin(\theta)$ for $\theta_0 = \pm\pi$ and $\theta_f = 0$, where $\epsilon \approx -\frac{\nu\Omega}{2\sqrt{2}}t^2$. Thus, by encompassing the intersection even just barely, we have achieved a non-trivial geometric phase.

We also noted that there are symmetries maintained throughout the evolution by choosing this path. In particular, the quantity $L_z + \frac{1}{2}\sigma_z$ is conserved throughout the evolution, something that cannot be said about the natural adiabatic evolution choice. This means that the evolution cannot make transitions between eigensupaces that do not share this value. We believe this helps maintain adiabatcity despite a much shorter evolution time.

Based on classical simulations with $\Omega = 2\pi \times 10$ kHz and $\nu = 2\pi \times 3$ kHz, we found that if we take 25 ms as an appropriate amount of time to evolve the state using the natural evolution choice, and we compare that to the same evolution method but with only 330 μs to evolve, the fidelity between the two is about 80%. If we instead use the symmetric method explained here, the same evolution time gives us a fidelity of over 96%.

For completeness, we compared three different evolutions via classical simulation. The first is the planned evolution with the ideal Hamiltonian and the conical intersection are present. The simulation is for 10 ms, and the final state is shown in Supplementary Fig.2a. In the evolution represented by Supplementary Fig.2b, halfway through we switched to the Hamiltonian $H(t) = \nu n_x + \nu n_y - \frac{\Omega(t)}{2}\sqrt{(a_x + a_x^\dagger)^2 + (a_y + a_y^\dagger)^2}$, which does not have a conical intersection, but has the same adiabatic potential energy surface as the lower half of the ideal Hamiltonian. As can be seen, the geometric phase is less present. Finally, in Supplementary Fig.2c we used the non-CI Hamiltonian the whole evolution, and there is no sign of geometric phase interference.

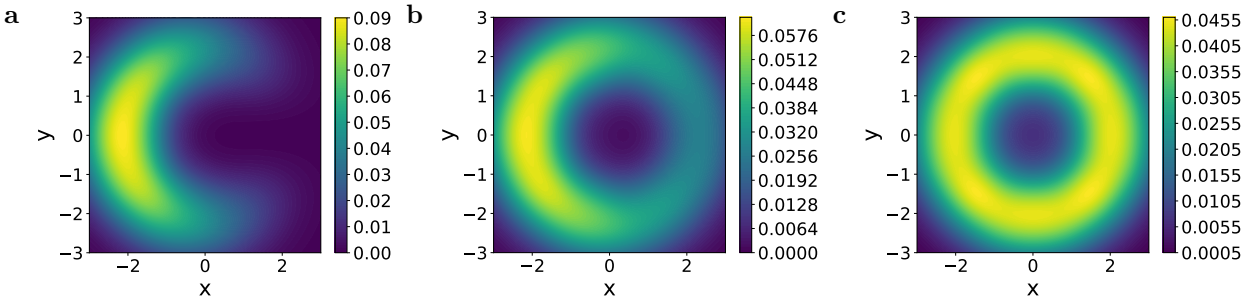

Supplementary Fig. 1: **a**, Simulation results of adiabatic evolution when CI is present, where $\Omega = 2\pi \times 10$ kHz and $\nu = 2\pi \times 3$ kHz for both modes, and the simulation lasts 10 ms. **b**, Same simulation results, but switching to the non-CI Hamiltonian midway through the evolution. The geometric phase interference is less prominent. **c**, Using the non-CI Hamiltonian the whole way through. There is no sign of geometric phase interference. Slight difference in outermost points most likely stem from non-adiabatic behavior when switching Hamiltonians.

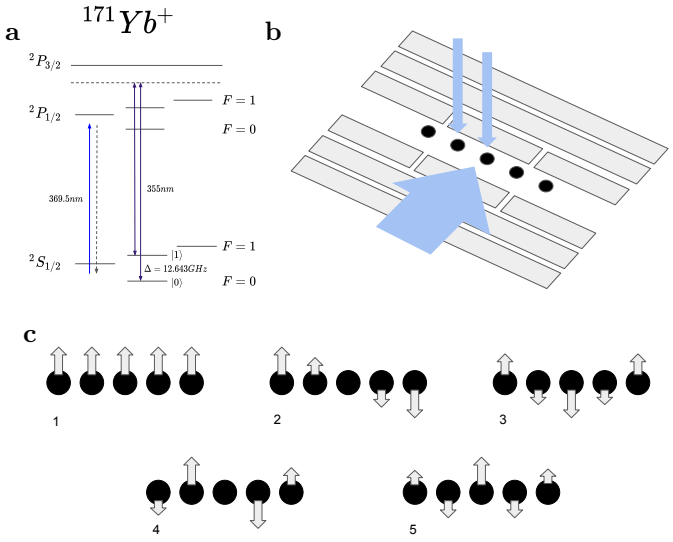

Supplementary Fig. 2: **a**, Important energy levels for cooling, detection, and Raman transitions in $^{171}\mathrm{Yb}^+$. **b**, Layout of surface trap, five ions, global Raman beam, and individual addressing Raman beams in experimental setup. **c**, Relative coupling into the motional modes by each ion, in order of descending resonant frequency [2, 3]. The ions we used were the center one for simulation, and one of its nearest neighbors for measurement. The motional modes we used were the third and the fifth (also known as the zig-zag mode).

Supplementary Material References

[1] Leibfried, D., Blatt, R., Monroe, C. & Wineland, D. Quantum dynamics of single trapped ions. *Rev. Mod. Phys.* **75**, 281 (2003).

[2] Jia, Z. *et al.* Determination of multimode motional quantum states in a trapped ion system. *Phys. Rev. Lett.* **129**, 103602 (2022).

[3] Debnath, S. *A programmable five qubit quantum computer using trapped atomic ions.* Ph.D. thesis, University of Maryland, College Park (2016).

[4] Roos, C. F. Ion trap quantum gates with amplitude-modulated laser beams. *New J. Phys.* **10**, 013002 (2008).

[5] Wineland, D. J. *et al.* Experimental primer on the trapped ion quantum computer. *Prog. Phys.* **46**, 363–390 (1998).

[6] Wineland, D. J. *et al.* Experimental issues in coherent quantum-state manipulation of trapped atomic ions. *Journal of research of the National Institute of Standards and Technology* **103**, 259 (1998).